https://doi.org/10.5194/gmd-2023-105
Preprint. Discussion started: 31 May 2023

Geoscientific Model Development Discussions

Developing meshing workflows for Geologic Uncertainty Assessment in High-Temperature Aquifer Thermal Energy Storage

Ali Dashti[1], Jens C. Grimmer[1], Christophe Geuzaine[2], Florian Bauer[3], Thomas Kohl[1]

[1]Institute of Applied Geosciences, Karlsruhe Institute of Technology (KIT), Karlsruhe, Germany
[2]Université de Liège, Institut Montefiore B28, 4000 Liège, Belgium
[3]Institute for Nuclear Waste Disposal, Karlsruhe Institute of Technology (KIT), Hermann-von-Helmholtz-Platz 1, 76344 Eggenstein-Leopoldshafen, Germany

Correspondence to: Ali Dashti (Ali.dashti@kit.edu)

Abstract. Evaluating uncertainties of geological features on temperature and pressure changes in reservoir's fluids are crucial for a safe and sustainable operation of the High-Temperature Aquifer Thermal Energy Storage (HT-ATES). This study uses a new automated surface fitting function in Python API of GMSH (v. 4.11) to model the impact of arbitrary structural barriers and variations of roof and floor geometries on temperature and pressure in heat storage application. A workflow is developed in Python to implement an automated mesh generation routine for varying geological scenarios that cannot be predicted by surface-based exploration methods. This way, the geologic models and their underlying uncertainties are transferred into reservoir simulations. We applied our modelling approach on two case studies: 1) Greater Geneva Basin with the Upper Jurassic ("Malm") limestone reservoir of 100 m thickness and 2) the DeepStor project in the Upper Rhine Graben with an Oligocene sandstone reservoir of 10 m thickness. In the Greater Geneva Basin showcase, the upper and lower surfaces of the reservoir are shifted ± 8 and ± 10 m, respectively to perturb topology of the thick reservoir. Independence of the heat plume from reservoir´s topology indicates the limited propagation of the induced thermal regime in thick reservoirs and redundancy of the advanced exploration campaigns like 3D seismic. In DeepStor, an arbitrary sub-seismic fault juxtaposing the permeable sandstone layers against low-permeable clay-marl units is introduced to the base case model. The arbitrary fault is located in distances varying 4 m to 118 m from the borehole and resulted in a ~10% difference in the pressure field of the cases. Modelling the pressure and temperature in the tilted reservoir reveals that heat tends to accumulate updip while pressure values are higher in the downdip side.

Keywords: HT-ATES, GMSH, Greater Geneva Basin, DeepStor, geological uncertainty, numerical modelling

1 Introduction

Aquifer Thermal Energy Storage (ATES) yields the highest storage capacities compared to other energy storage solutions (Fleuchaus et al., 2018). Based on the injection temperature and application, ATES falls into two categories: I) High-Temperature (>50 °C) Aquifer Thermal Energy Storage (HT-ATES; e.g. Wesselink et al. (2018) and II) Low-Temperature Aquifer Thermal Energy Storage (LT-ATES; e.g. Réveillère et al. (2013).

https://doi.org/10.5194/gmd-2023-105
Preprint. Discussion started: 31 May 2023

Geoscientific Model Development Discussions

Seasonal storage constitutes a low risk in terms of time, budget and performance (Fleuchaus et al., 2020a). The typically applied "huff-puff" concept of HT-ATES foresees the horizontal transport of large volumes of fluid within an aquifer. HT-ATES offers the major advantage to be less site-dependent compared to conventional deep geothermal utilizations. It exploits suitable aquifers that can be encountered in the deeper subsurface of major populated urban areas (Schmidt et al., 2018; Mahon et al., 2022). Appropriate reservoir conditions for heat storage are widely distributed in the topmost 2 km of the Earth´s continental crust (Bloemendal et al., 2014; Gao et al., 2019; Dinkelman and van Bergen, 2022; Fleuchaus et al., 2020a; Pasquinelli et al., 2020). Suitable reservoirs for thermal energy storage can also be found also in thick successions of fractured rocks (e.g. Birdsell and Saar (2020)). As another advantage, HT-ATES's requires small surface area comprising an asset in populated urban zones (Böhm and Lindorfer, 2019).

A successful design of a HT-ATES depends on appropriate petrophysical properties of the deep aquifer that can be used as a reservoir. Such design requires conceptual and numerical models. Most studies on HT-ATES describe reservoir geometries as homogeneous km-large, box shaped volumes. The sensitivity of these volumes to relevant parameters (e.g. well configuration, transmissivity, flow rate, conductivity, …) has been intensively studied (Stricker et al., 2020; Green et al., 2021; Mindel and Driesner, 2020; Fleuchaus et al., 2020a; Fleuchaus et al., 2020b). The conceptual designs of both, HT- and LT-ATES, typically apply box shaped reservoir simulations while ignoring natural geometries and impact of geological uncertainties.

Establishing HT-ATES in previously exploited oil fields benefits from data and experiences acquired during previous exploration and production. Some previously exploited hydrocarbon reservoirs are re-used for natural gas storage to back up higher demand during winter season. In terms of heat storage, these reservoirs have not yet been used and this lack of experience requires the need for numerical modelling approaches.

Subsurface data inevitably encompass different levels of uncertainty originating from measurement errors, biased extrapolations and interpretations, heterogeneities, and simplifications (Caers, 2011; Wellmann and Regenauer-Lieb, 2012; Wellmann et al., 2010). In this study we focus on the impact of structural and geometrical uncertainties on pressure and temperature distribution and their spatio-temporal development in heat storage reservoirs during operation. These uncertainties comprise varying topologies of reservoir roof and floor surfaces and sub-seismic faults that laterally delimit the reservoir, but cannot be predicted from surface measurements. These impacts are commonly simplified or ignored due to complex re-meshing process in numerical analyses. Advancement in geological uncertainty studies are starting to be transferred into numerical simulations (Dashti et al., 2023). Prognostic geological models cannot cope with the uncertainties of the subsurface. Uncertainty analysis points to the necessity of applying stochastic geological models rather than a deterministic geometrical representation. This study extends the application presented by Dashti et al. (2023) on an automated workflow to transfer stochastic structures from geological uncertainty models to a fast and reliable numerical meshing tool that allows the quantification of the relevant processes in HT-ATES.

In this study, two candidates for HT-ATES in the vicinity of populated areas are evaluated: 1) the Greater Geneva Basin (GGB) next to Geneva (Switzerland; Collignon et al. (2020) and 2) the DeepStor site, located at the Campus of Karlsruhe

https://doi.org/10.5194/gmd-2023-105
Preprint. Discussion started: 31 May 2023


Geoscientific Model Development Discussions

Institute of Technology (KIT). These two locations differ strongly by their reservoir morphology, lithology, petrophysical properties, and thicknesses for HT-ATES. For both the Geneva and DeepStor HT-ATES cases we have investigated the impact of structural uncertainties, i.e. accuracy of geological data, on them by designing different scenarios. Quantification of the uncertainty included thickness and topology variations by adapting a fast, specific meshing workflow. The meshing routine generates surfaces from point clouds in order to create arbitrary shaped volumes with topologies derived from 3D seismic analyses. The meshing procedure allows to establish various stochastic numerical models that account for the resolution of the data and even can include for additional fault zones. This way, meshing routines represent the basis for advanced thermohydraulic analyses from arbitrarily inserted faults into the model.

2 Uncertainty and Numerical model developments

2.1 Greater Geneva Basin

A proposed HT-ATES system in the outskirt of Geneva is located in the Greater Geneva Basin (GGB) and is supposed to be charged by surplus 35 GWh from a nearby power plant (Collignon et al., 2020). For details on the geology of the GGB see Kuhlemann and Kempf (2002). Two formations are recognized as potential heat storage reservoirs: thick Upper Jurassic Malm limestones and thin sand-rich layers in the Cenozoic Molasse sediments (Chelle-Michou et al., 2017). The geothermal gradient for the GGB comprises 25-30 K/km (Rybach, 1992; Chelle-Michou et al., 2017). The 2530 m deep geothermal well (Thonex-01) intersected >900 m thick Malm limestones and marl succession with a bottom hole temperature of 88 °C and low flow rates of <0.5 l/s (Guglielmetti et al., 2022). The geothermal gradient is not very promising for geothermal heat production from the reservoir, but heat storage can efficiently support the higher heat demand during the winter season.

Collignon et al. (2020) published a local parametric sensitivity analysis on Molasse and Malm limestone reservoirs of the HT-ATES. The proposed target Malm limestones are considered to consist of patch reefs with high porosities (Chevalier et al., 2010; Rybach, 1992). In their scope study, Collignon et al. (2020) assumed a box shaped reservoir with flat surfaces at the depths of -1100 and -1200 m. We investigate the impact of the geological uncertainty caused by the carbonate reservoir on pressure and temperature. Such uncertainty typically originate from the exploration of a reservoir structure that is based on earlier seismic data acquisition (Feng et al., 2021; Faleide et al., 2021). The sources of error comprise data acquisition, availability of borehole data for depth calibration, quality of velocity models for time-depth conversion, ambient noise level (Bond, 2015).

To perturb the geological model, a randomized noise is superposed on the upper and lower surfaces of the reservoir layer that are assumed to be inverted from 3D seismic data. A surface can be considered as discrete points in x, y and z coordinates of a 3D space. For the Malm limestone reservoir a grid of points (representing surfaces) is generated. The regular grid consists of 41×26 nodes in x and y directions, respectively with a fixed 20 m distance. The perturbed model is a purely generic example where at each grid point the random noise is added to its vertical coordinate. The base case of this study corresponds to the reference model of Collignon et al. (2020). Figure 1 presents a scenario with two perturbed surfaces

https://doi.org/10.5194/gmd-2023-105
Preprint. Discussion started: 31 May 2023

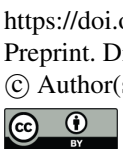

Geoscientific Model Development Discussions

of the Malm limestone layer. Figure 1-a shows roughness and irregularity of the reservoir's surfaces. For the top surface, a range of ± 8 m noise is imposed on the primary flat plane. For the bottom surface the range of perturbation increased to ± 10 m due to the decrease in the quality of seismic data with depth. The whole discretized model (Figure 1-b) includes basement, reservoir and caprock as lower, middle and upper units, respectively.

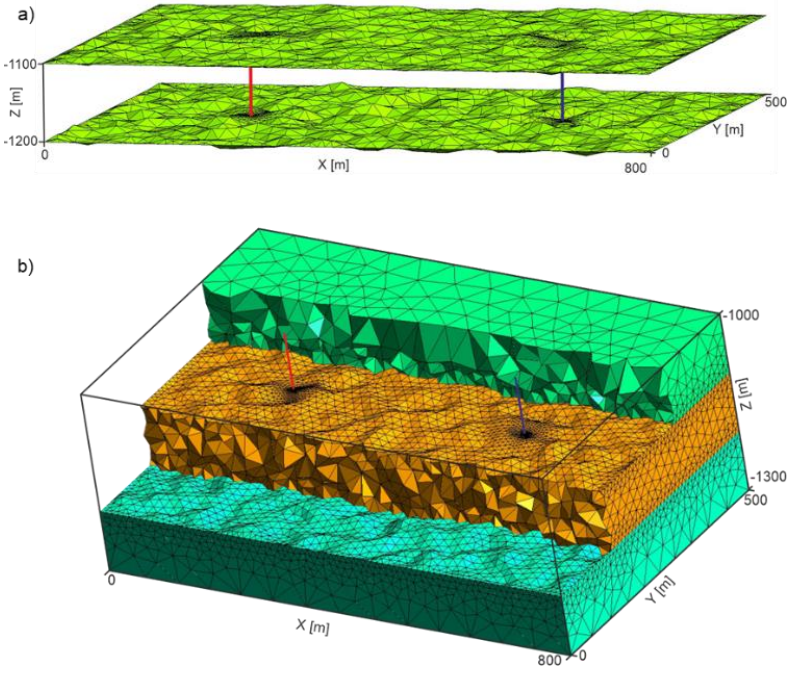

Figure 1: a) Randomly perturbed top and bottom surfaces of the Malm limestone reservoir. b) The whole discretized model of a perturbed scenario. The reservoir layer in the middle is sandwiched by the basement and caprock units. Red line represents the warm well whereas the cold well is shown with the blue line in both subplots.

2.2 Greater Geneva Basin

The proposed DeepStor site is located in the Cenozoic sediments of the Upper Rhine Graben (URG) and intended to use an abandoned oil field for thermal storage in the sand layers of the Oligocene Meletta beds. For details on the geology and stratigraphy of the URG see Grimmer et al. (2017), Dèzes et al. (2004) and Schumacher (2002) and references therein. Figure 2 highlights the abundance of the normal faults in the URG that – if suitably oriented in the stress field – facilitate convective fluid flow in fractured Permo-Mesozoic and crystalline basement rocks. The convective regime builds positive thermal anomalies in the Cenozoic graben filling sediments locally with gradients of up to 100 K/km (Agemar et al., 2012; Baillieux et al., 2013; Pribnow and Schellschmidt, 2000). DeepStor HT-ATES targets the Oligocene Meletta sandstones that exploited for oil production from 1957 to 1986 (Reinhold et al., 2016) in the footwall of the sealing Leopoldshafen fault where oil and some gas accumulated updip (Wirth, 1962; Böcker et al., 2017).

https://doi.org/10.5194/gmd-2023-105
Preprint. Discussion started: 31 May 2023

Geoscientific Model Development Discussions

The DeepStor model in this study comprises a volume of 1000×1000 m^2 area and 250 m thickness (see Figure 3-a with the sand layers of the Meletta beds). Due to the overall uncertainty, sub-seismic faults characterized by offsets <20 m cannot be properly identified neither by the 3D-seismic data nor from borehole data and laterally delimit thin reservoir layers impacting heat storage potentials and operation (Glubokovskikh et al., 2022). In order to cope with these structural uncertainties, mathematical models have been developed to characterize these faults due to their abundance and importance (Gong et al., 2019; Rotevatn and Fossen, 2011; Harris et al., 2019; Damsleth et al., 1998). Fractal theory is applied to predict the number, strike length and throw of sub-seismic faults by extrapolating the power-law distribution derived from properties of the identified faults (Wang et al., 2018; Hooker et al., 2014; Twiss and Moores, 2006). Hence, sub-seismic faults are expected, but their location in the subsurface remains largely unknown.

In order to evaluate the impact of sub-seismic faults on HT-ATES operation, an arbitrary N-S-striking fault is introduced in different parts of the basic geological model. Strike of this arbitrary fault is parallel with Stutensee and Leopoldshafen faults (Figure 2). The dip-slip displacement of the introduced sub-seismic fault is as large as the thickness of the reservoir and therefore treated as a lateral seal. Hence, our modelling results also apply for faults with larger dip-slip displacements. The single test well (a warm one) is positioned in the center of the model (Figure 3). The data from this well is later on processed to establish a possible relation between measured pressure values and location of a sealing fault. This way, the DeepStor model is more similar to real storage cases where a test well allows for an optimum design. This test well is supposed to act as the warm well in the future. The fault has moved 16 times around the well in order to quantify its impact on temperature and pressure in the reservoir through thermohydraulic simulations. The borehole and fault are modelled as vertical line and plane, respectively. In total 17 scenarios are considered:

- Fourteen scenarios with a fault varying from 4 m to 112 m distances east of the well
- Two scenarios with a fault in the west of the well at 8 and 48 m distances
- One fault-free base case

Figure 3-b represents a scenario with a possible location of the arbitrary fault at 98 m distance in the east of the well.

https://doi.org/10.5194/gmd-2023-105
Preprint. Discussion started: 31 May 2023

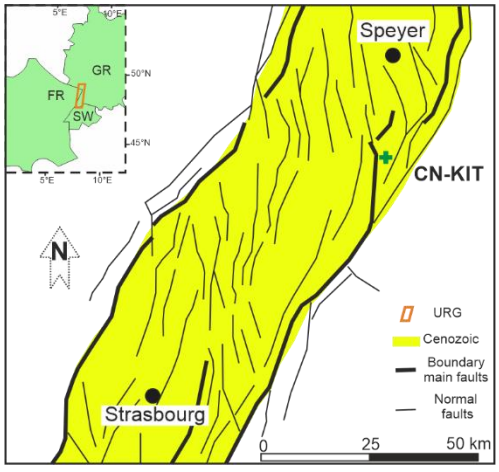

Figure 2: A tectonic overview of the URG and its surrounding area. The green plus symbol indicates the proposed location for HT-ATES in the north of Karlsruhe. Bold lines mark major faults of the rift boundary fault system. DeepStor site is located between Leopoldshafen (in west) and Stutensee (in east) normal faults (modified from Grimmer et al. (2017)).

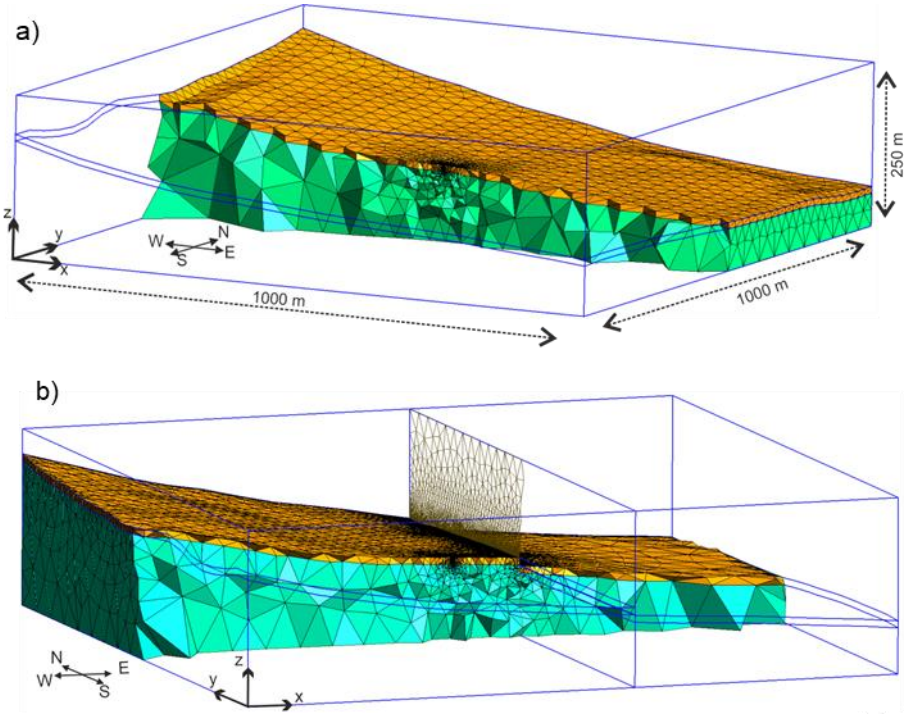

Figure 3: a) A section across the permeable reservoir layer (orange) and impermeable host rocks (green) of the DeepStor base case. Impermeable caprock is not shown to have a better view on the spatially discretized model and topology of the thin reservoir layer. b) A sealing fault is introduced in the model. Dimension of the faulted model remains the same as the base case represented in subplot a (1000×1000×250). Fault surface of this example is located 98 m east of the well.

https://doi.org/10.5194/gmd-2023-105
Preprint. Discussion started: 31 May 2023


Geoscientific Model Development Discussions

2.3 Tool developments based on GMSH

The open source finite element mesh generator GMSH (Geuzaine and Remacle, 2009) is used to generate the required high quality spatial discretization. GMSH recently gained the ability to create geometrical surfaces passing through arbitrary sets of points and to combine these surfaces with other geometrical entities (curves, surfaces or volumes) through Boolean operations thanks to the built-in OpenCASCADE geometry kernel (Open CASCADE Technology). The new features linked to B-Spline surface interpolation and non-manifold meshing are available in the latest stable version of GMSH (v. 4.11). This allows to preserve the geological topology of the layers and enables the generation of high quality, adapted finite element meshes for complex geometries like modified Malm limestone reservoir surfaces (Figure 1) or thin, tilted Meletta beds (Figure 3). While the model of Dashti et al. (2023) lacks complicated geometries, the recently added functionality of GMSH is tested in this study by implementing complex topologies. The overall workflow for the spatial discretization is based on the following steps that are implemented in a template script using Python API of GMSH (see code availability section):

- The global outline of the domain of study is defined by adding a single (solid) volume – usually a parallelepiped;
- Geological layers are defined by fitting, through numerical optimization, a B-Spline surface going through each set of data points defining a geological interface. The point cloud can come from any modelling tool and the only requirement is that they should make a regular grid. Default parameters for the B-Spline degree and the tolerances for the fitting ensure a smooth surface with reasonable local curvature changes;
- Sources and wells (or other zero- or one-dimensional features) are defined as additional points and curves in the model;
- All the geometrical entities are intersected globally in order to produce a conforming boundary representation of the complete model, possibly with non-manifold features (points and curves “embedded” in surfaces and/or volumes);
- The link between geometrical entities and physical properties is established using representative points;
- Mesh size fields are automatically defined to refine the mesh when approaching the boundaries of the reservoir, as well as when approaching the wells and/or the sources;

The global unstructured mesh is then generated automatically. The mesh is made of tetrahedra inside volumes, triangles on the interfaces, lines on the wells and points on the sources. This mesh is conforming, i.e. the elements are arranged in such a way that if two of them intersect, they do so along a face, an edge or a node, and never otherwise. It is necessary to first generate the desired number of scenarios for uncertainty analysis and later on one single block of code in Python will yield the same number of meshes.

A multi-level mesh refinement in both models is carried out through several available functions in GMSH. In the case of GGB, Distance and Threshold fields allowed for a gradual mesh size increase of 2 m to 75 m from the boreholes toward the boundaries of the model. In the adjacency of the Malm’s contacts also mesh size was set to be 15 m while it increases up to 75 m. In total, GGB meshes have an average of 35'000 nodes and 210'000 elements. The average is presented here because

https://doi.org/10.5194/gmd-2023-105
Preprint. Discussion started: 31 May 2023


Geoscientific Model Development Discussions

from scenario to scenario, the mesh is different due to topological variations. The fast and automated workflow allows for generating a mesh in a complicated geological model like the perturbed scenarios of GGB in 80 sec running on a Core i7 laptop. Noteworthy, running time includes the whole process from importing the data into GMSH up to exporting a refined conforming mesh. For DeepStor also the same refinement strategies but with different mesh sizes are used. Minimum mesh size is set to be 0.5 m close to the single borehole while it gradually increases to 125 m. The model contains also a large fault plane making the mesh more complex. Distance and Threshold fields are introduced for the fault plane forcing the mesh size to be 3 m in the immediate vicinity of the fault. The base case of the DeepStor does not include the fault plane and the number of nodes and elements are 9'026 and 62'317, respectively. In the base case of DeepStor the mesh is generated in 45 sec. For other 16 scenarios with the sub-seismic fault, the number of nodes and elements increase to 37'000 and 250'000, respectively. To achieve mentioned mesh sizes in both the GGB and DeepStor cases, a mesh sensitivity analysis was performed to guarantee independence of simulation results (temperature and pressure fields) from the mesh size.

2.4 Numerical modelling

The open source finite element application TIGER (Thermo-Hydro-Chemical sImulator for Geoscience Research) (Gholami Korzani et al., 2020) is used to simulate the heat storage processes for GGB and DeepStor cases. TIGER is developed on top of the MOOSE (Multiphysics Object-Oriented Simulation Environment) framework. The MOOSE framework is fully coupled and encompasses a wide variety of completely implicit solvers (Lindsay et al., 2022; Gaston et al., 2009). It inherits functionalities of PETSc (a suite of data structures and routines applied for the scalable parallel solution) and libMesh libraries. In our study the coupled thermal and hydraulic kernels of the TIGER are deployed to obtain the evolution of temperature and pressure. TIGER simplifies the meshing by enabling a mixed-dimensional problem formulation. In GMSH the connection of lower and higher dimensional elements is implemented so straightforward that can be achieved quickly.

Used thermal and petrophysical data for simulation of both cases are directly coming from the published models. Table 1 contains the values selected for required parameters in our simulations. Collignon et al. (2020) used MATLAB Reservoir Simulation Toolbox but in this study, TIGER is used for simulation and results (heat plume propagation and recovery) are compared and benchmarked based on their work. The GGB model includes a doublet system simulated in a 10-year time scheme. Loading, unloading and resting phases of the model follow the strategy introduced by Collignon et al. (2020). Each annual cycle includes four months of loading, two months of rest, four months of unloading, and two months of rest. The loading phase corresponds to the injection of hot water via the warm well when the cold well is under production. Temperatures for hot and cold fluid injection are set to be 90 °C and 39 °C. Both wells have a fixed flow rate of 10 l/s but in different directions. The time stepping for 10 years of simulation is divided into 10 loading, 10 unloading and 20 rest phases. The piecewise linear function of MOOSE is used to increase the time steps in each phase. In the loading and unloading phases time steps increase from 1 hour to 10 days from the start time to the last day. For the rest periods the time stepping increases from 1 hour to 20 days. For GGB the run time of each simulations is around 3 hours on 12 cores of a high-performance computing (HPC) cluster.

https://doi.org/10.5194/gmd-2023-105
Preprint. Discussion started: 31 May 2023


Geoscientific Model Development Discussions

Stricker et al. (2020) introduced properties of the reservoir for DeepStor in a generic model and we used the data of their reference case (Table 1). In our simulations the geology and consequently the mesh is the major difference to the model of Stricker et al. (2020) while petrophysical parameters remain the same. The simulation time is set to 10 years. Rather than the doublet model described by Stricker et al. (2020), a single "huff-puff" well is demonstrated in our study. The hot fluid with 140 °C temperature is injected in a six-month period and during the subsequent six months the well produces the previously injected, i.e. stored, hot water. The flow rate is fixed to be 2 l/s in both the injection and production phases. In reality a second well will be needed to compensate for the fluid volumes. Herein we are focusing on the thermohydraulic impacts in the near field of a well and our model works with a single well scenario. The time discretization follows the six-month cycles and consists of 20 temporal frames for the whole simulation time. Time steps increase from 10 minutes to 10 days in each cycle. Time steps at the start point of each cycle are considered to be shorter in DeepStor model compared to GGB due to the lower thickness of the reservoir and higher complexity of the model. Almost 74'000 degrees of freedom in the faulted scenarios demands for an average of 4 hours computation time on 12 cores of a HPC cluster. Simulations in the faulted scenarios of the DeepStor are computationally more demanding compared to GGB due to the complexity of the model.

For both the GGB and DeepStor cases, similar strategies applied for defining boundary and initial conditions. After running a steady state thermohydraulic simulation for each scenario, the results have been applied as the initial condition for that specific case. In other words, 17 steady state models are calculated for the DeepStor and each one is used as the initial condition of the transient simulation. Two boundary conditions are also applied for the temperature variable at the top and bottom surfaces of each model. By introducing a function representing the temperature gradient, MOOSE allows for assigning the correct temperature values to the top and bottom surfaces of the model. The function is mentioned in the following:

$$T = T_{surface} + z \times GT, \quad (1)$$

where z denotes the depth (in m) and GT the geothermal gradient (in K/km). In the case of pressure, one boundary condition is defined on the bottom surface of the model based on the following function:

$$P = (z - WT) \times \rho \times g, \quad (2)$$

where WT represents water table, ρ is the density (in kg/m^3) and g is the gravitational acceleration (set as 9.81 m/s^2).

https://doi.org/10.5194/gmd-2023-105
Preprint. Discussion started: 31 May 2023

Table 1: Parameters selected as inputs from the numerical simulations of two case studies.

Parameter		Case studies	
		GGB (Collignon et al., 2020)	DeepStor (Stricker et al., 2020)
Reservoir	Thickness [m]	~ 100	10
	Permeability [m^2]	9.8×10^{-15}	6.6×10^{-14}
	Porosity [-]	0.15	0.15
	Thermal conductivity [W/mK]	1.8	2.5
Caprock	Thickness [m]	~ 100	~ 100
	Permeability [m^2]	9.8×10^{-19}	10^{-18}
	Porosity [-]	0.05	0.15
	Thermal conductivity [W/mK]	1.4	1.4
Flow rate [l/s]		10	2
Geothermal gradient [K/km]		26	50
Water table [m]		10	10

3 Results

3.1 GGB

The upper and lower contacts of the reservoir are perturbed to investigate their possible effect/s on the heat and pressure distributions in the HT-ATES. Heat recovery of the system has not been affected due to its dependence on local temperature values. Despite changing the topology of the reservoir, propagation of the heat also looks the same for three presented scenarios in Figure 4. Temperature values of the highlighted traces in Figure 4 are extracted to visualize the heat plume propagation. The uppermost scenario in Figure 4 is the base case (a box shaped reservoir with flat planes) while the two next ones are named scenarios 1 and 2 in Figure 5. Even after 10 years the heat is still locally propagated around the warm well for the base case and other two perturbed scenarios (Figure 5). Overlap of all three curves confirms the independence of the temperature field from introduced topological perturbation of the thick reservoir layer. Heat plumes (Figure 4) and the curves (Figure 5) are slightly asymmetric due to the effect of the cold well. During the injection of hot fluid in warm well, cold well is in production phase that pulls the hot fluid from the warm well toward itself.

https://doi.org/10.5194/gmd-2023-105
Preprint. Discussion started: 31 May 2023

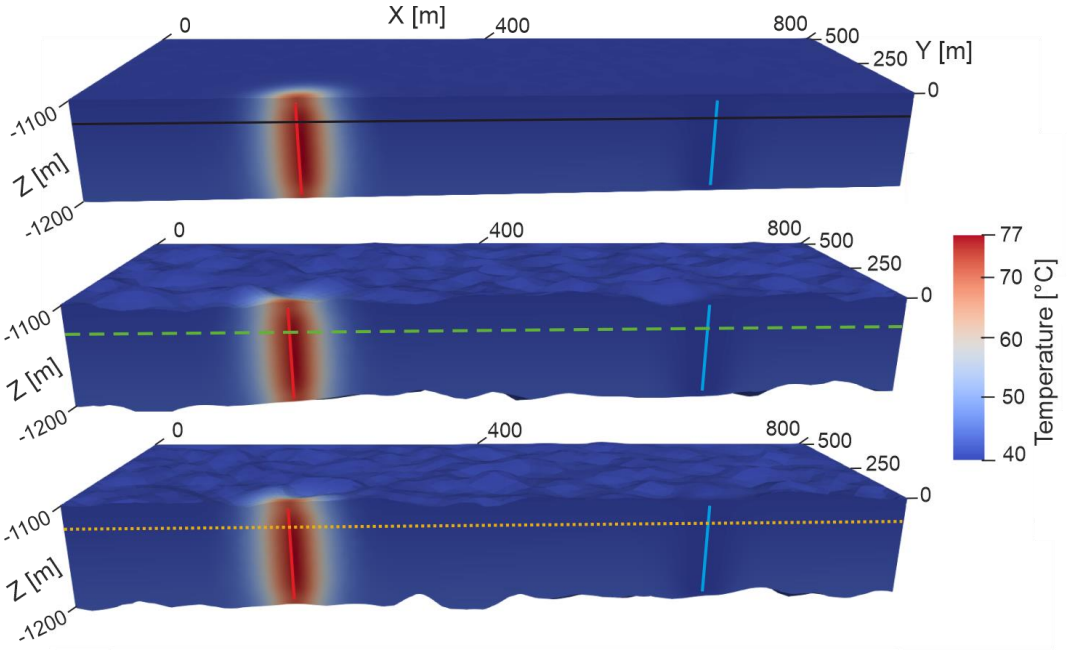

Figure 4: Heat distribution after 10 years of storage in the Malm limestone reservoir of the GBB. Red and blue lines represent warm and cold wells, respectively. The upper scenario with a uniform box shaped reservoir is considered as the base case while contacts of the reservoir in the middle and lower scenarios are perturbed and irregular. Solid black, dashed green and dotted orange traces are used in Figure 5 for plotting the temperature values.

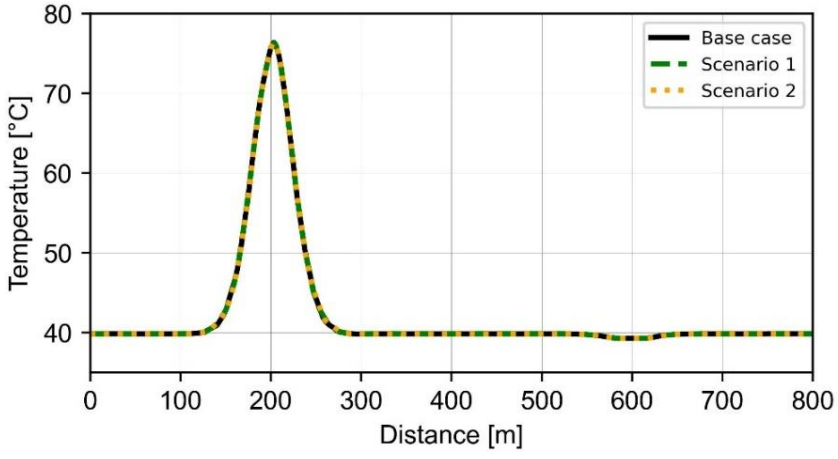

Figure 5: Temperature distribution curves of the values coming from the base case and two perturbed scenarios after 10 years of injection and production for the GGB. Warm and cold wells are located at 200 m and 600 m points of the x axis. To find the location of the plotted trace, refer to Figure 4. Similar to the models' extension in x direction x axis i.e. Distance (in m) ranges from 0 m to 800 m.

https://doi.org/10.5194/gmd-2023-105
Preprint. Discussion started: 31 May 2023

Geoscientific Model Development Discussions

3.2 DeepStor

For HT-ATES infrastructure, the real underground topology of the target storage reservoir (sand layers in Meletta beds) is simulated. In spite of including the real geology of the reservoir in this study, both the recovery and heat plume radius of the base case are similar to what is presented by Stricker et al. (2020) for their reference case. As Figure 6 shows, heat recovery of the system increases from 67% to more than 82% from the first to the tenth year. The recovery rate is calculated as the ratio between extracted and injected thermal energy at the top of the well's openhole section. The difference between 17 simulated cases is negligible (~2%). Cases with the highest difference i.e. extremes are plotted in Figure 6 to keep the plot readable. Meanwhile, the recovery difference of scenarios increases through the time as three recovery curves are diverging. Despite the negligible difference, the case where fault is located 48 m in the west of the well has the best performance while the case with fault in 4 m distance in the east shows the worst. For the best recovery, the reason is linked to the total volume of the reservoir and upward movement of the low-density hot fluid. The reservoir is tilted and hot fluids move updip due to the density effect. A sealing fault in 48 m distance from the injection point will keep the hot fluid within the confined reservoir. The reason behind the worst recovery is that the arbitrary fault affects the heat plume and results in heat loss.

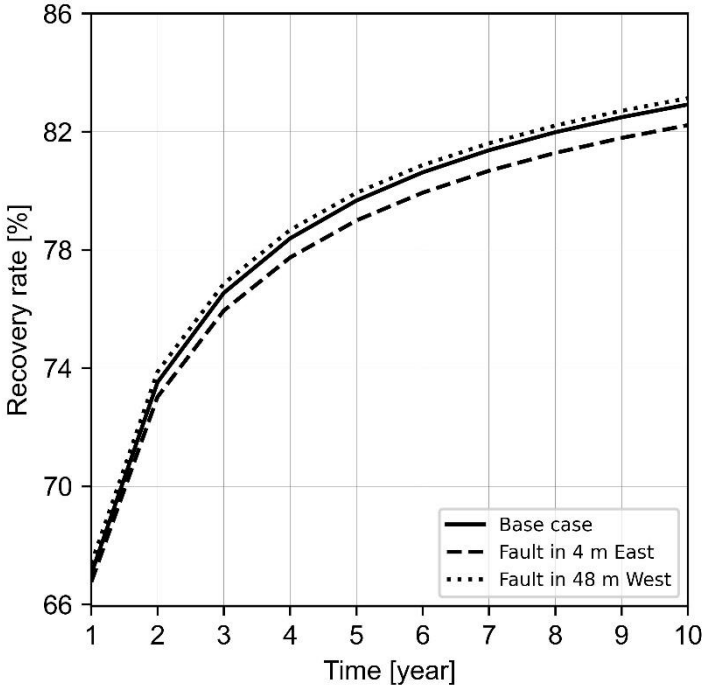

Figure 6: Heat recovery in three scenarios of the DeepStor model. Only two extremes and the base case are plotted to keep the plot more readable.

Figure 7 shows the heat accumulation in four different simulated scenarios. In the base case (Figure 7-a), size and temperature of heat plume confirms the results of Stricker et al. (2020). The plume extends about 45 m in x and y directions.

https://doi.org/10.5194/gmd-2023-105
Preprint. Discussion started: 31 May 2023


Geoscientific Model Development Discussions

The only difference is that here the slope of the plume follows the tilted reservoir. The angle between the vertical borehole and tilted heat plumes in Figure 7 indicates this 5° inclination. Based on size of the heat plume, it is highly unlikely to see any effect of Leopoldshafen or Stutensee faults on the thermal performance of the system in a 10-year time period. The heat plume is affected in the most severe case where the arbitrary fault is supposed to be only 4 m in the east of well (Figure 7-b). Moving the fault on the edge of the plume (45 m in the east: Figure 7-c), the heat plume looks almost similar to the base case. Similarity of Figure 7-a and c suggests the disappearance of the sealing fault's impact on the heat plume. Surprisingly, the heat plume is getting slightly warmer when the fault is assumed to be 48 m in west side of the well (Figure 7-d). Recovery curves also confirmed the slightly higher efficiency of this scenario. After injecting hot water, it flows toward the updip direction of the reservoir due to its lower density. Then, a sealing fault in the western side can prevent the flow of hot fluid from moving farther. In a 10-year simulation time, such localization of the reservoir can increase the performance but in a longer period these barriers reduce the available storage space of the reservoir.

https://doi.org/10.5194/gmd-2023-105
Preprint. Discussion started: 31 May 2023

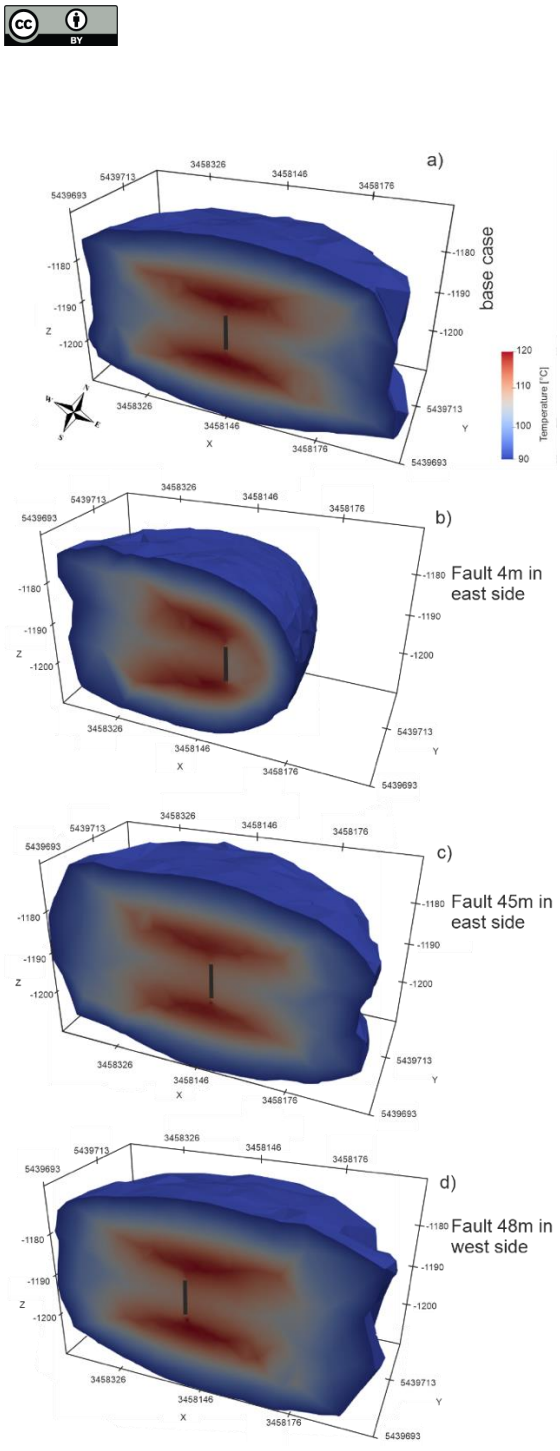

Figure 7: Heat accumulation in four different scenarios of the DeepStor model. Planned well is shown as a solid black line. Subplots from a to d represent different scenarios including base case, arbitrary fault in 4 and 45 m in the east of the well and 48 m in the west. Temperature scale is also the same and shown only once in subplot a to avoid repetition.

An unpredicted sealing fault in the system where fluids are injected continuously may increase the pressure values dramatically. Figure 8-a and b show a 2D section of the model and the total pressure (hydrostatic plus operation-caused

https://doi.org/10.5194/gmd-2023-105
Preprint. Discussion started: 31 May 2023


Geoscientific Model Development Discussions

pressure) values across the sand reservoir after the first injection cycle. Ten injection (and production) cycles are included in the simulation and the maximum pressure increase is observed at the end of first one. The plotted trace of the pressure in Figure 8-b is shown as a dash dotted line in Figure 8-a. The plotted pressure curves illustrate the data of four cases (to keep the figure readable) and initial condition of the trace passing through the reservoir. The pressure increase of base case at the borehole location is about 10% (from ~ 11.52 to 12.61 MPa). Initial condition of the model shows that pressure values is distributed asymmetrically in the reservoir. It confirms the role of layers' inclination on pressure distribution. Eastern parts of the reservoir layer is dipping downward and under higher hydrostatic pressures. The pressure curve of the base case also indicates this fact by its asymmetric shape that shows a higher pressure accumulation in the eastern part of the model. This behaviour of the pressure is in contradiction to temperature that was accumulating upward. Therefore, in majority of the faulted scenarios (14 out of 16), the arbitrary fault is located in the eastern side of the well to present the worst-case scenarios enabling a better assessment of the highest possible pressure increase. Figure 8-b suggests also a relation between the pressure increase and distance of the fault. Fault surface acts as a barrier along which pressure accumulates. Even in the worst-case scenario (fault is 4 m in the east of the well) the pressure value at the sealing fault is only 7% higher than the value in the same location of the base case. The total pressure at the fault location of worst-case (4 m) is 13.1 MPa while in base case it is 12.25 MPa. Note the 4 m value on the x axis of Figure 8-b to extract pressure values for the worst and base cases.

Figure 9 is a contour plot of the total pressure distribution within the reservoir layer. A surface parallel to the tilted reservoir layer is chosen to make this plot. The trace line shown in Figure 8-a is extended in y direction to be converted from a line to a surface and applicable for the contour plots. In both plots, the well is located in the center with 0.0 and 0.0 coordinates. The first notable point is that pressure is accumulating alongside of the sealing fault surface. Instead of spherical pressure plumes, contour lines are proposing an elliptical high-pressure regime with major axis perpendicular to the faults surface. Despite the negligible difference in the faults' distance between Figure 9-a and b, the pressure values are obviously higher in the case with a fault in eastern side of the well.

https://doi.org/10.5194/gmd-2023-105
Preprint. Discussion started: 31 May 2023

Geoscientific Model Development Discussions

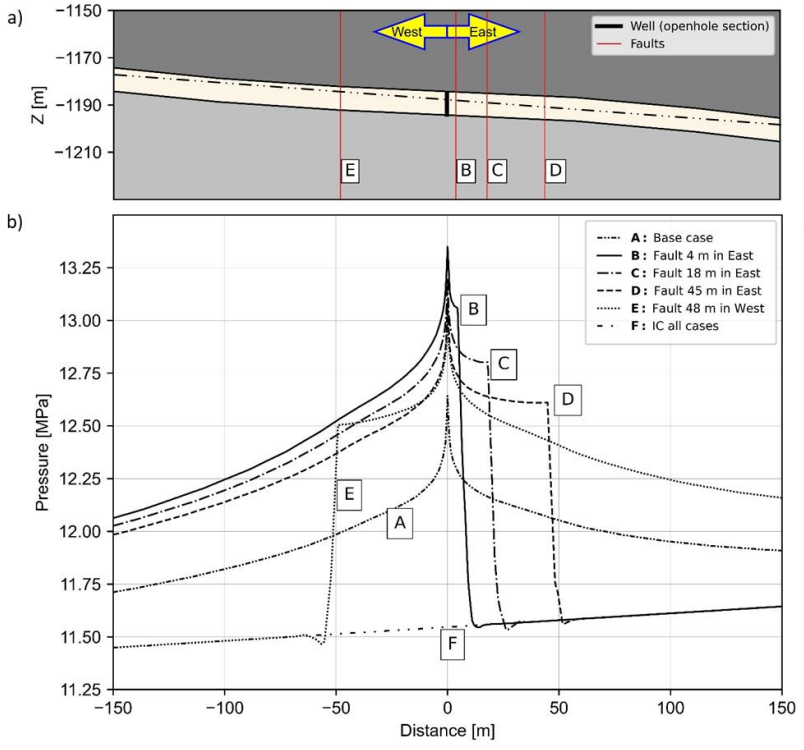

Figure 8: Total pressure increase of five simulated cases at the end of the first injection cycle. The cross section in subplot a indicates the position of the traces used for plotting the pressure data of five different scenarios and the initial condition (IC). Negative values for distance represent the western side of the well. To make the curves more readable, scenarios are labelled as A, B, C, D, E and the initial condition as F. This way, a visual correlation can be easily established from subplot a to b.

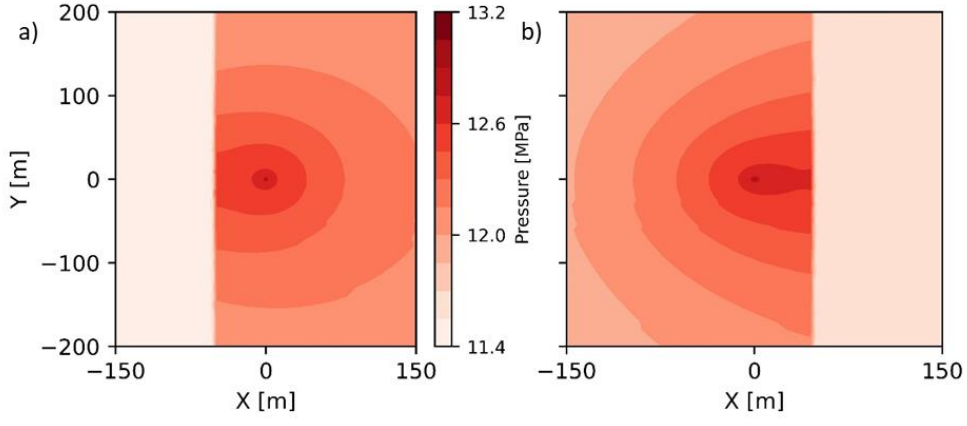

Figure 9: Total pressure changes after the first injection cycle in two scenarios. The well position is in the center of both plots (coordinates=0.0 and 0.0). Fault position is easily distinguishable by the sharp change in the pressure data: 48 m in the west of well (a) and 45 m in the east (b). Negative and positive values for x and y axis are relative to the position of the well.

https://doi.org/10.5194/gmd-2023-105
Preprint. Discussion started: 31 May 2023


Geoscientific Model Development Discussions

4 Discussion

The meshing workflow introduced here facilitates including real geological models and their uncertainties. Meshing is a cumbersome step in between geological models and numerical simulators. Herein highly complicated reservoir topologies are meshed fast and efficiently without any manual manipulation. Generation of complex surfaces, mesh refinement, embedment, and physical properties attribution are all automated for any number of cases. The automated workflow then exports as much as required stochastic geological meshes to cover a range of the uncertainties. This study used generic initial models and introduced arbitrary uncertainties to them but developed workflow can be deployed for real world cases and uncertainties coming from any type of data. Now, the geological models and their uncertainty can be transferred directly into reservoir simulations. This geological uncertainty later on can be applied in both the exploration and development phases. First, geologically uncertain simulations decipher the sensitivity of the results (temperature, pressure, displacement, etc.) to the perturbed parameters (boundaries of the reservoir in the GGB and location of the sub-seismic fault in the DeepStor). Second, the relation between distribution of properties and topology of layers can raise the importance of including real geology for the development plans. Third, in case of establishing a relation between the perturbed parameters and their outcomes, more scenarios can be generated to broaden the range of uncertainty. This relation can be later on used to update the prior knowledge based on the collected data during the operation.

4.1 Exploration campaign design

GGB case was provided in this study with the purpose of detecting the possible impacts of topological uncertainty on the HT-ATES's thermal performance. Results confirmed that heat propagation even after 10 years of continuous injection and production is still about 40 m around the hot well in the thick reservoir. Upper and lower surfaces of the reservoir are also hardly playing any role in the heat distribution of the thick Malm reservoir. In contrary to this conclusion, Dashti et al. (2023) confirmed the dependence of the underground flow properties on location of the small structural elements in geological models. In the case of thin reservoirs (<20 m) also a ±10 m shift can increase/decrease the volume of the reservoir up to 50%, but thermal performance of the Malm reservoir in GGB is independent of such small scale thickness variations. This fact confirms the unnecessity of complex and time-consuming exploration methods for those cases. Efforts for a 3D seismic campaign can intensify the exploration phase. Dedicating huge efforts to preliminary steps discourages policy makers from investing in renewable solutions like HT-ATES. The GGB case clearly demonstrated that even a rough estimation of the underground surfaces is reliable enough for predicting the behaviour of the thick reservoirs at least for a 10-year snapshot. Even existing 2D seismic slices of oilfields can bring enough accuracy for generating reliable forecasts in cases like GGB. Computationally affordable geological scenario-based analyses of geological boundaries can save the time dedicated to exploration.

https://doi.org/10.5194/gmd-2023-105
Preprint. Discussion started: 31 May 2023


Geoscientific Model Development Discussions

4.2 Field development plan

Based on presented results for DeepStor, distribution of both the heat and pressure are tightly linked to the inclination of the thin reservoir. Therefore, including this real model besides its uncertainty, e.g. perturbing the layer's inclination, can be a key factor in an optimum planning for the second borehole. In case of drilling the cold well with a 500 m distance from warm one, the negligible 5° inclination can make a 45 m difference between the depth of a horizontal and a tilted layer. As the next step, perturbing the angle and topology of the layer can provide us with a range of possible depths that can be expected during the drilling of the second borehole.

In the URG, the majority of hydrocarbons are accumulated thanks to the existence of sealing faults. Therefore, DeepStor can also encounter these structural features. Thermohydraulic simulations revealed only if the fault be located in the distances less than the heat plume radius (45 m), can affect the storage success. Target sand layer is a very thin and in the case of thicker formations, effect of the faults can be even less important and observable.

The arbitrary sealing fault in DeepStor model is detectable in the calculated pressure values from the top of the well. Figure 10 is a plot representing history of the total pressure values on the openhole section during first year of HT-ATES. A correlation between fault distance from the well and pressure increase can be detected in this figure. Meanwhile, locating the fault in the east (downdip of the reservoir) or west (updip) makes a difference. Fault distance in two scenarios is the same (8 m) but in different directions from the well. Due to the pressure accumulation in the downdip, a fault with the same distance in the eastern side of the well can increase pressure more than the same one in the western side. The slight difference between solid black curve and dashed red curves is detectable in Figure 10.

The observable trend in Figure 10 enables a primary forecast of fault distance (in case of having any) merely based on the recorded pressures from the borehole. The pressure difference between the day five of injection and initial condition versus the distance of the fault to well are used to formulate the forecast. It is assumed that in the day five of injection the initial reservoir condition and injection operation have reached to an equilibrium. This pressure value can also be achieved through operating a separate hydraulic test on the well. In the base case of DeepStor the maximum total pressure reaches from the initial 11.5 MPa to 13.3 MPa, i.e. 15% increase, at the end of injection cycle. Meanwhile, in the day five more than half of this increase (11.5 MPa to 12.5 MPa) is observed. Figure 11 shows the relation of these two variables where fault's distance from the well versus the pressure increase after five days are plotted. All the 14 black dots represente the scenarios in which fault is located in the east of the well. For a comparison, the case with a fault in 8 m distance in west of the well is also plotted as a circle to present the pressure accumulation in the downdip. To address the worst-case scenarios, the forecast has been founded on the base of the faults locating in the east side of the well. A simple exponential function with three degrees of freedom provides an acceptable level of accuracy (RMSE=0.013 MPa) for the prediction. In the case of having more simulations, the function can be updated to be more robust. However, we here merely try to present the possibility of formulating such simple forecast systems in a complicated reservoir. More advanced methods like machine learning can also increase the accuracy of the prediction. Then, other arbitrary distances can be fed into the predictor and pressure value in the

https://doi.org/10.5194/gmd-2023-105
Preprint. Discussion started: 31 May 2023

Geoscientific Model Development Discussions

day five of injection will be returned without making meshes and running the numerical simulation. Meanwhile, after running the test phase and measuring pressure in the day five of injection, the data can be inserted into the predictor to back-calculate the distance of the fault (in case of existing). In the case of finding discrepancies between prior assumptions about the fault's distance with output of the predictor, the geologic model can be updated. Validity of this inversion scheme strongly depends on the accuracy of material properties. Otherwise, the difference between measured and calculated pressures can originate from any other source like petrophysical properties.

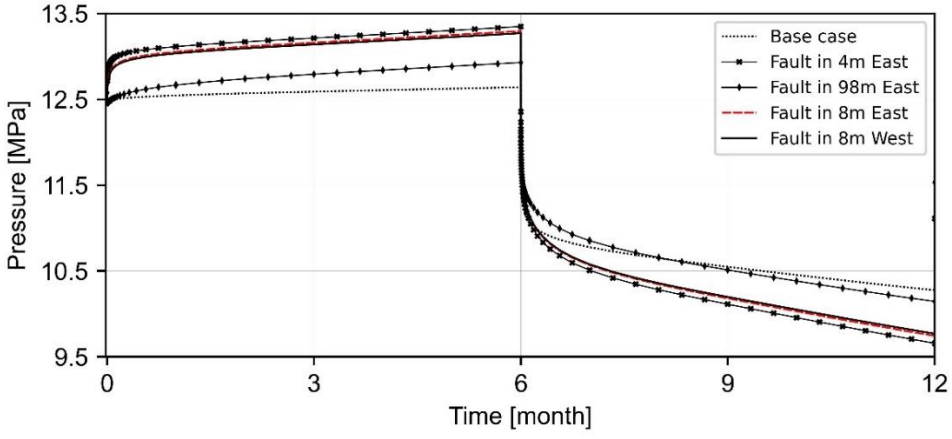

Figure 10: Total pressure evolution in the well during the first injection and production phase. Only five cases are plotted to keep the figure readable. Higher pressure accumulation in the east of the well can be observed by the slight difference between dashed red (Fault in 8m East) and black (Fault in 8m West) curves.

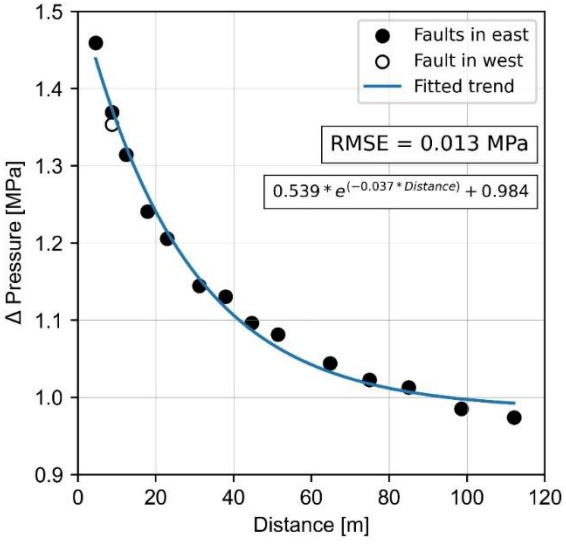

Figure 11: Difference between borehole pressure on day five of injection and initial condition (Δ Pressure) versus the distance of the arbitrary fault to borehole. The continuous line is representing an exponential function with three degrees of freedom.

https://doi.org/10.5194/gmd-2023-105
Preprint. Discussion started: 31 May 2023


Geoscientific Model Development Discussions

5 Conclusion

In the frame of uncertainty quantification, we have developed a tool applicable for complex geological structures. This study demonstrates a geological scenario based analysis of HT-ATES in two showcases. A new implementation in the GMSH provided us with the possibility of recreating real geological surfaces automatically rather than a manual time demanding process. The developed automated workflow in Python allows making several meshes composed of surfaces with arbitrary shapes. The workflow also enables a fast generation of a myriad of watertight finite element meshes in one single run of a Python script. Generated meshes will link geological uncertainty of the models to numerical simulators. We proposed the geological uncertainty as a key input for decision-making later in different phases of the HT-ATES study ranging from exploration to development.

A HT-ATES is simulated for Geneva as the second most populated city in Switzerland. In the GGB model, random geological topologies are generated to assess the sensitivity of results with respect to the underground topology. Falling from other side of the roof in exploration plans happens when redundant levels of accuracy are demanded. GGB model clarifies this fact by showing the independence of the temperature from geometry of the thick reservoir. The Malm layer with 100 m thickness can be detected even through 2D seismic slices and surveys for finding the exact topology of the top and bottom surfaces with higher accuracies are unnecessary. This study highlights the necessity of running computationally affordable simulations prior to any exploration campaign.

The porous sand layers existing within Meletta beds beneath KIT campus are also a promising storage space. For DeepStor adding one more level of complexity (a sealing sub-seismic fault) to interpreted data expresses the performance risks i.e. possible significant heat losses and/or pressure increase. Presented evaluation on DeepStor proved that only in cases where a sealing fault is closer than 45 m to the well, the thermal performance of the system can be affected. The effect on the thermal recovery of borehole is hardly observable but the overall dimension of the heat plume can change due to such faults in the vicinity (<45 m). Numerically calculated pressure values at the borehole location can decipher the faults even in 118 m distances. Relation between pressure changes and location of the introduced sealing fault is used in this study to establish a forecast scheme for detecting possible locations of the barriers in the DeepStor model. Meanwhile, adjacency of the proposed site to oil-depleted reservoirs is a big advantage but the real experience of HT-ATES in such locations is still immature, hence first-order estimates from risk analyses need to be conducted. Further studies are required to address also the challenges associated to DeepStor including the geochemical interaction or the impact of residual hydrocarbons in the formation.

Code and data availability. GMSH can be accesses via the published releases on the official GitLab repository at https://gitlab.onelab.info/gmsh/gmsh. Required data and developed workflow for running the model for one of the showcases (GGB) is fully documented and available in the GitHub

(https://github.com/Ali1990dashti/GeoMeshPy/tree/main/Examples/Storage%20Model) and Zenodo (https://zenodo.org/record/7643506#.Y-znA3bMKUl) repositories of the first author.

Author contributions. AD: Conceptualization; Methodology; Simulation; Validation; Code development; Writing– original draft. JCG: Conceptualization; Geological modelling; Supervision; review & editing. CG: Code development; Writing – review & editing. FB: Geological modelling; TK: Conceptualization; Supervision; Writing – review & editing

Competing interests. The authors declare that they have no conflict of interest.

Acknowledgements. Ali Dashti is receiving the financial support from The German Academic Exchange Service (Deutscher Akademischer Austauschdienst: DAAD) to do his PhD in Germany as the Research Grants-Doctoral programmes in Germany 2019/20. This organization is appreciated for giving the opportunity to researchers. The study is also part of the Helmholtz portfolio project Geoenergy. The support from the program "Renewable Energies", under the topic "Geothermal Energy Systems", is gratefully acknowledged. Authors appreciate the support of Prof. Eva Schill (eva.schill@kit.edu) for the data availability and geological model of the DeepStor. Dr. Denise Degen (denise.degen@cgre.rwth-aachen.de) is appreciated due to her support and constructive comments. Fruitful comments of Kai R. Stricker (kai.stricker@kit.edu) regarding the numerical modelling section are wholeheartedly acknowledged.

6 References

Agemar, T., Schellschmidt, R., and Schulz, R.: Subsurface temperature distribution in Germany, Geothermics, 44, 65–77, https://doi.org/10.1016/j.geothermics.2012.07.002, 2012.

Baillieux, P., Schill, E., Edel, J.-B., and Mauri, G.: Localization of temperature anomalies in the Upper Rhine Graben: insights from geophysics and neotectonic activity, International Geology Review, 55, 1744–1762, https://doi.org/10.1080/00206814.2013.794914, 2013.

Birdsell, D. T. and Saar, M. O.: Modeling Ground Surface Deformation at the Swiss HEATSTORE Underground Thermal Energy Storage Sites, 22046, 2020.

Bloemendal, M., Olsthoorn, T., and Boons, F.: How to achieve optimal and sustainable use of the subsurface for Aquifer Thermal Energy Storage, Energy Policy, 66, 104–114, https://doi.org/10.1016/j.enpol.2013.11.034, 2014.

Böcker, J., Littke, R., and Forster, A.: An overview on source rocks and the petroleum system of the central Upper Rhine Graben, Int J Earth Sci (Geol Rundsch), 106, 707–742, https://doi.org/10.1007/s00531-016-1330-3, 2017.

Böhm, H. and Lindorfer, J.: Techno-economic assessment of seasonal heat storage in district heating with thermochemical materials, Energy, 179, 1246–1264, https://doi.org/10.1016/J.ENERGY.2019.04.177, 2019.

Bond, C. E.: Uncertainty in structural interpretation: Lessons to be learnt, Journal of Structural Geology, 74, 185–200, https://doi.org/10.1016/j.jsg.2015.03.003, 2015.

Caers, J.: Modeling Uncertainty in the Earth Sciences, John Wiley & Sons, Ltd, Chichester, UK, 2011.

https://doi.org/10.5194/gmd-2023-105
Preprint. Discussion started: 31 May 2023

Chelle-Michou, C., Do Couto, D., Moscariello, A., Renard, P., and Rusillon, E.: Geothermal state of the deep Western Alpine Molasse Basin, France-Switzerland, Geothermics, 67, 48–65, https://doi.org/10.1016/j.geothermics.2017.01.004, 2017.

Chevalier, G., Diamond, L. W., and Leu, W.: Potential for deep geological sequestration of CO2 in Switzerland: a first appraisal, Swiss J Geosci, 103, 427–455, https://doi.org/10.1007/s00015-010-0030-4, 2010.

Collignon, M., Klemetsdal, Ø. S., Møyner, O., Alcanié, M., Rinaldi, A. P., Nilsen, H., and Lupi, M.: Evaluating thermal losses and storage capacity in high-temperature aquifer thermal energy storage (HT-ATES) systems with well operating limits: insights from a study-case in the Greater Geneva Basin, Switzerland, Geothermics, 85, 101773, https://doi.org/10.1016/j.geothermics.2019.101773, 2020.

Damsleth, E., Sangolt, V., and Aamodt, G.: Sub-seismic Faults Can Seriously Affect Fluid Flow in the Njord Field off Western Norway - A Stochastic Fault Modeling Case Study, in: All Days, New Orleans, Louisiana, 9/27/1998 - 9/30/1998, 1998.

Dashti, A., Gholami Korzani, M., Geuzaine, C., Egert, R., and Kohl, T.: Impact of structural uncertainty on tracer test design in faulted geothermal reservoirs, Geothermics, 107, 102607, https://doi.org/10.1016/j.geothermics.2022.102607, 2023.

Dèzes, P., Schmid, S. M., and Ziegler, P. A.: Evolution of the European Cenozoic Rift System: interaction of the Alpine and Pyrenean orogens with their foreland lithosphere, Tectonophysics, 389, 1–33, https://doi.org/10.1016/j.tecto.2004.06.011, 2004.

Dinkelman, D. and van Bergen, F. (Eds.): Evaluation of the country-wide potential for High-Temperature Aquifer Thermal Energy Storage (HT-ATES) in the Netherlands, 2022.

Faleide, T. S., Braathen, A., Lecomte, I., Mulrooney, M. J., Midtkandal, I., Bugge, A. J., and Planke, S.: Impacts of seismic resolution on fault interpretation: Insights from seismic modelling, Tectonophysics, 816, 229008, https://doi.org/10.1016/j.tecto.2021.229008, 2021.

Feng, R., Grana, D., and Balling, N.: Uncertainty quantification in fault detection using convolutional neural networks, GEOPHYSICS, 86, M41-M48, https://doi.org/10.1190/geo2020-0424.1, 2021.

Fleuchaus, P., Schüppler, S., Bloemendal, M., Guglielmetti, L., Opel, O., and Blum, P.: Risk analysis of High-Temperature Aquifer Thermal Energy Storage (HT-ATES), Renewable and Sustainable Energy Reviews, 133, 110153, https://doi.org/10.1016/j.rser.2020.110153, 2020a.

Fleuchaus, P., Schüppler, S., Godschalk, B., Bakema, G., and Blum, P.: Performance analysis of Aquifer Thermal Energy Storage (ATES), Renewable Energy, 146, 1536–1548, https://doi.org/10.1016/j.renene.2019.07.030, 2020b.

Fleuchaus, P., Godschalk, B., Stober, I., and Blum, P.: Worldwide application of aquifer thermal energy storage – A review, Renewable and Sustainable Energy Reviews, 94, 861–876, https://doi.org/10.1016/j.rser.2018.06.057, 2018.

Gao, L., Zhao, J., An, Q., Liu, X., and Du, Y.: Thermal performance of medium-to-high-temperature aquifer thermal energy storage systems, Applied Thermal Engineering, 146, 898–909, https://doi.org/10.1016/j.applthermaleng.2018.09.104, 2019.

Gaston, D., Newman, C., Hansen, G., and Lebrun-Grandié, D.: MOOSE: A parallel computational framework for coupled systems of nonlinear equations, Nuclear Engineering and Design, 239, 1768–1778, https://doi.org/10.1016/j.nucengdes.2009.05.021, 2009.

Geuzaine, C. and Remacle, J.-F.: Gmsh: A 3-D finite element mesh generator with built-in pre- and post-processing facilities, Int. J. Numer. Meth. Engng., 79, 1309–1331, https://doi.org/10.1002/nme.2579, 2009.

Gholami Korzani, M., Held, S., and Kohl, T.: Numerical based filtering concept for feasibility evaluation and reservoir performance enhancement of hydrothermal doublet systems, Journal of Petroleum Science and Engineering, 190, 106803, https://doi.org/10.1016/j.petrol.2019.106803, 2020.

Glubokovskikh, S., Saygin, E., Shapiro, S., Gurevich, B., Isaenkov, R., Lumley, D., Nakata, R., Drew, J., and Pevzner, R.: A Small CO 2 Leakage May Induce Seismicity on a Sub-Seismic Fault in a Good-Porosity Clastic Saline Aquifer, Geophys. Res. Lett., 49, https://doi.org/10.1029/2022GL098062, 2022.

Gong, L., Liu, B., Fu, X., Jabbari, H., Gao, S., Yue, W., Yuan, H., Fu, R., and Wang, Z.: Quantitative prediction of sub-seismic faults and their impact on waterflood performance: Bozhong 34 oilfield case study, Journal of Petroleum Science and Engineering, 172, 60–69, https://doi.org/10.1016/j.petrol.2018.09.049, 2019.

Green, S., McLennan, J., Panja, P., Kitz, K., Allis, R., and Moore, J.: Geothermal battery energy storage, Renewable Energy, 164, 777–790, https://doi.org/10.1016/j.renene.2020.09.083, 2021.

Grimmer, J. C., Ritter, J. R. R., Eisbacher, G. H., and Fielitz, W.: The Late Variscan control on the location and asymmetry of the Upper Rhine Graben, Int J Earth Sci (Geol Rundsch), 106, 827–853, https://doi.org/10.1007/s00531-016-1336-x, 2017.

Guglielmetti, L., Heidinger, M., Eichinger, F., and Moscariello, A.: Hydrochemical Characterization of Groundwaters' Fluid Flow through the Upper Mesozoic Carbonate Geothermal Reservoirs in the Geneva Basin: An Evolution more than 15,000 Years Long, Energies, 15, 3497, https://doi.org/10.3390/en15103497, 2022.

Harris, R., Bracken, K., Miller, B., Angelovich, S., and O'Toole, T.: Subseismic Fault Identification Using the Fault Likelihood Attribute: Application to Geosteering in the DJ Basin, in: Proceedings of the 7th Unconventional Resources Technology Conference, Denver, Colorado, USA, 7/22/2019 - 7/24/2019, 2019.

Hooker, J. N., Laubach, S. E., and Marrett, R.: A universal power-law scaling exponent for fracture apertures in sandstones, Geological Society of America Bulletin, 126, 1340–1362, https://doi.org/10.1130/B30945.1, 2014.

Kuhlemann, J. and Kempf, O.: Post-Eocene evolution of the North Alpine Foreland Basin and its response to Alpine tectonics, Sedimentary Geology, 152, 45–78, https://doi.org/10.1016/S0037-0738(01)00285-8, 2002.

Lindsay, A. D., Gaston, D. R., Permann, C. J., Miller, J. M., Andrš, D., Slaughter, A. E., Kong, F., Hansel, J., Carlsen, R. W., Icenhour, C., Harbour, L., Giudicelli, G. L., Stogner, R. H., German, P., Badger, J., Biswas, S., Chapuis, L., Green, C., Hales, J., Hu, T., Jiang, W., Jung, Y. S., Matthews, C., Miao, Y., Novak, A., Peterson, J. W., Prince, Z. M., Rovinelli, A., Schunert, S., Schwen, D., Spencer, B. W., Veeraraghavan, S., Recuero, A., Yushu, D., Wang, Y., Wilkins,

A., and Wong, C.: 2.0 - MOOSE: Enabling massively parallel multiphysics simulation, SoftwareX, 20, 101202, https://doi.org/10.1016/j.softx.2022.101202, 2022.

Mahon, H., O'Connor, D., Friedrich, D., and Hughes, B.: A review of thermal energy storage technologies for seasonal loops, Energy, 239, 122207, https://doi.org/10.1016/j.energy.2021.122207, 2022.

Mindel, J. and Driesner, T.: HEATSTORE: Preliminary Design of a High Temperature Aquifer Thermal Energy Storage (HT-ATES) System in Geneva Based on TH Simulations, 2020.

Open CASCADE Technology, https://www.opencascade.com.

Pasquinelli, L., Felder, M., Gulbrandsen, M. L., Hansen, T. M., Jeon, J.-S., Molenaar, N., Mosegaard, K., and Fabricius, I. L.: The feasibility of high-temperature aquifer thermal energy storage in Denmark: the Gassum Formation in the Stenlille structure, bgsd, 68, 133–154, https://doi.org/10.37570/bgsd-2020-68-06, 2020.

Pribnow, D. and Schellschmidt, R.: Thermal tracking of upper crustal fluid flow in the Rhine graben, Geophys. Res. Lett., 27, 1957–1960, https://doi.org/10.1029/2000GL008494, 2000.

Reinhold, C., Schwarz, M., and Perner, M.: The Northern Upper Rhine Graben re-dawn of a mature petroleum province?, https://doi.org/10.5169/seals-658196, 2016.

Réveillère, A., Hamm, V., Lesueur, H., Cordier, E., and Goblet, P.: Geothermal contribution to the energy mix of a heating network when using Aquifer Thermal Energy Storage: Modeling and application to the Paris basin, Geothermics, 47, 69–79, https://doi.org/10.1016/j.geothermics.2013.02.005, 2013.

Rotevatn, A. and Fossen, H.: Simulating the effect of subseismic fault tails and process zones in a siliciclastic reservoir analogue: Implications for aquifer support and trap definition, Marine and Petroleum Geology, 28, 1648–1662, https://doi.org/10.1016/j.marpetgeo.2011.07.005, 2011.

Rybach, L.: Geothermal potential of the Swiss Molasse basin, 1992.

Schmidt, T., Pauschinger, T., Sørensen, P. A., Snijders, A., Djebbar, R., Boulter, R., and Thornton, J.: Design Aspects for Large-scale Pit and Aquifer Thermal Energy Storage for District Heating and Cooling, Energy Procedia, 149, 585–594, https://doi.org/10.1016/j.egypro.2018.08.223, 2018.

Schumacher, M. E.: Upper Rhine Graben: Role of preexisting structures during rift evolution, Tectonics, 21, 6-1-6-17, https://doi.org/10.1029/2001TC900022, 2002.

Stricker, K., Grimmer, J. C., Egert, R., Bremer, J., Korzani, M. G., Schill, E., and Kohl, T.: The Potential of Depleted Oil Reservoirs for High-Temperature Storage Systems, Energies, 13, 6510, https://doi.org/10.3390/en13246510, 2020.

Twiss, R. J. and Moores, E. M.: Structural Geology, 2nd, W.H. Freeman, New York, NY, 2006.

Wang, X., Hou, J., Song, S., Wang, D., Gong, L., Ma, K., Liu, Y., Li, Y., and Yan, L.: Combining pressure-controlled porosimetry and rate-controlled porosimetry to investigate the fractal characteristics of full-range pores in tight oil reservoirs, Journal of Petroleum Science and Engineering, 171, 353–361, https://doi.org/10.1016/j.petrol.2018.07.050, 2018.

https://doi.org/10.5194/gmd-2023-105
Preprint. Discussion started: 31 May 2023

Wellmann, J. F. and Regenauer-Lieb, K.: Uncertainties have a meaning: Information entropy as a quality measure for 3-D geological models, Tectonophysics, 526-529, 207–216, https://doi.org/10.1016/j.tecto.2011.05.001, 2012.

Wellmann, J. F., Horowitz, F. G., Schill, E., and Regenauer-Lieb, K.: Towards incorporating uncertainty of structural data in 3D geological inversion, Tectonophysics, 490, 141–151, https://doi.org/10.1016/j.tecto.2010.04.022, 2010.

Wesselink, M., Liu, W., Koornneef, J., and van den Broek, M.: Conceptual market potential framework of high temperature aquifer thermal energy storage - A case study in the Netherlands, Energy, 147, 477–489, https://doi.org/10.1016/j.energy.2018.01.072, 2018.

Wirth, E.: Die Erdöllagerstätten Badens, Abh. Geol. Landesamt Baden-Württemberg: Freiburg, Germany, 4, 63–80, 1962.